

Infrared Corrections and Horizon Phase Transitions in Kaniadakis-Based Holographic Dark Energy

Manuel Gonzalez-Espinoza ^{1,*}, Samuel Lepe^{2,†}, Joel F. Saavedra ^{2,‡} and Francisco Tello-Ortiz ^{3,§}

¹*Laboratorio de investigación de Cómputo de Física, Facultad de Ciencias Naturales y Exactas, Universidad de Playa Ancha, Subida Leopoldo Carvallo 270, Valparaíso, Chile*

²*Instituto de Física, Pontificia Universidad Católica de Valparaíso, Casilla 4950, Valparaíso, Chile.*

³*Departamento de Ciencias Físicas, Universidad de La Frontera, Casilla 54-D, 4811186 Temuco, Chile.*

We study the cosmological and thermodynamic implications of holographic dark energy derived from the Kaniadakis deformation of the Bekenstein–Hawking entropy. Within a spatially flat FLRW background, the generalized entropy leads to an effective dark-energy density containing an infrared correction proportional to H^{-2} , modifying the dynamics of the apparent horizon. Using the Hayward–Kodama formalism, we obtain a geometric equation of state and perform a criticality analysis, revealing a Van der Waals–type structure with an inverted first-order phase transition and a non-physical swallowtail behavior in the Gibbs free energy, indicative of unstable thermodynamic branches. We further examine a dynamical extension including a \dot{H} contribution and show that the unconventional critical behavior persists. The phenomenological viability of the model is tested through a joint statistical analysis with cosmic chronometers, PantheonPlus Type Ia supernovae, and DESI baryon acoustic oscillation data. These results establish Kaniadakis holographic cosmology as a consistent framework linking generalized entropy, gravitational thermodynamics, and observationally viable dark-energy dynamics.

I. INTRODUCTION

Understanding the physical origin of dark energy and the mechanism driving late-time cosmic acceleration remains one of the most profound challenges in contemporary cosmology. Although the Λ CDM model provides an excellent phenomenological description of observational data—including CMB anisotropies [1], baryon acoustic oscillations [2], and Type Ia supernovae [3]—it leaves unresolved deep theoretical tensions. The cosmological constant problem highlights the enormous discrepancy between quantum vacuum energy estimates and the observed value [4], while the coincidence problem questions why dark energy and matter densities are of the same order precisely at the present epoch [5]. These conceptual issues strongly suggest that cosmic acceleration may reflect new gravitational or thermodynamic physics rather than a finely tuned vacuum energy.

Holographic dark energy (HDE) offers a compelling framework rooted in quantum gravity principles. Originally proposed by Li [6] and based on the holographic principle [7, 8], HDE relates the dark energy density to an infrared cutoff L through $\rho_{\text{de}} \propto L^{-2}$, using the Bekenstein–Hawking entropy relation $S = A/4$ [9, 10]. This construction naturally links ultraviolet and infrared scales and yields an effective equation of state parameter close to $w \simeq -1$, in agreement with observations.

However, the classical area law is expected to receive corrections from quantum, statistical, or gravitational

effects near Planck scales. This expectation has motivated the exploration of generalized entropy formalisms, including Tsallis [11], Rényi [12], Barrow [13], and Kaniadakis entropies [14, 15]. Among these, the Kaniadakis entropy is particularly well suited for relativistic systems, as it emerges from κ -deformed statistics consistent with Lorentz symmetry and introduces a single deformation parameter K while preserving a consistent thermodynamic structure.

When implemented holographically in a cosmological setting¹, the Kaniadakis entropy modifies the standard HDE density by introducing an additional contribution proportional to $K^2 H^{-2}$. This correction generates enhanced infrared sensitivity, significantly affecting both the background expansion and the effective dark energy equation of state $w_{\text{de}}(z)$. More importantly, it modifies the thermodynamic properties of the apparent horizon—the natural causal boundary in FLRW cosmology—through its influence on the Hayward–Kodama surface gravity [18, 19] and the Misner–Sharp quasi-local energy [20].

The thermodynamic interpretation of gravity provides the natural theoretical framework to investigate these modifications. Following the foundational works of Bekenstein and Hawking [9, 10], Jacobson demonstrated that Einstein’s equations can be derived from the Clausius relation $\delta Q = T\delta S$ applied to local Rindler horizons [21]. Complementary formulations based on the unified first law and apparent horizon thermodynamics were developed by Hayward and others [19]. These results establish that the interplay between spacetime geometry

*Electronic address: manuel.gonzalez@upla.cl

†Electronic address: samuel.lepe@pucv.cl

‡Electronic address: joel.saavedra@pucv.cl

§Electronic address: francisco.tello@ufrontera.cl

¹ See [16, 17] for related cosmological analyses in the Kaniadakis setting.

and thermodynamics is not accidental but reflects a fundamental property of gravitational dynamics.

From an observational standpoint, any viable modification of holographic dark energy must confront high-precision late-time data. Cosmic chronometers provide direct reconstructions of $H(z)$ from differential galaxy ages [22, 23], the PantheonPlus sample delivers improved Type Ia supernova constraints over a broad redshift range [24], and the latest BAO measurements from DESI DR2 further tighten constraints on the expansion history [25, 26]. Since entropic deformations typically manifest as infrared corrections, they become dynamically relevant at low redshift, although degeneracies with Λ CDM may persist at the homogeneous level [27, 28]. A consistent assessment therefore requires both thermodynamic consistency and systematic observational confrontation.

Motivated by these considerations, in this work we present a comprehensive analysis of Kaniadakis holographic cosmology. First, we derive the effective equation of state of the apparent horizon, $P = P(v, T)$, directly from the unified first law without invoking the quasi-static approximation, uncovering a nontrivial critical structure. Second, we contrast this framework with alternative infrared prescriptions, particularly the Granda-Oliveros cutoff [29], which provides a local reformulation of HDE. Remarkably, we find that the Kaniadakis deformation induces an inverted first-order phase transition in the Gibbs free energy $G(T, P)$, reflected in the non-monotonic behavior of the P - v diagram in horizon thermodynamics.

The manuscript is organized as follows. In Sect. II the holographic dark energy model is presented. The Sect. III introduces the apparent horizon dynamics and in Sect. IV presents the equation of state. Sect. V is devoted to a detailed thermodynamic analysis of the system. By imposing the standard criticality conditions. In Sect. VI we investigate the classical stability of the model through the effective sound speed. Sect. VII derives the modified background dynamics and obtains explicit expressions for the Hubble expansion rate. These results provide the basis for the observational analysis presented in Sect. VIII, where the model is confronted with late-time cosmological probes through a joint statistical analysis employing cosmic chronometers, the PantheonPlus Type Ia supernova sample, and baryon acoustic oscillation measurements from DESI. Finally, Sect. IX summarizes the main results and discusses their implications for holographic cosmology. Technical derivations and complementary analyzes are presented in Appendices A, B and C.

Throughout the manuscript the mostly positive signature is used $-, +, +, +$, and units where $8\pi G = c = 1$.

II. KANIADAKIS ENTROPY AND ITS HOLOGRAPHIC FORMULATION

The statistical foundation of the Kaniadakis entropy stems from a relativistic generalization of Boltzmann-Gibbs theory [14, 15]. Unlike other non-additive entropies such as Tsallis or Rényi, the Kaniadakis deformation preserves fundamental structures of special relativity by introducing a κ -deformed exponential and logarithm constructed to remain invariant under Lorentz transformations. The entropy functional

$$S_K = - \int d\Gamma f \ln_{\kappa} f, \quad (1)$$

where \ln_{κ} denotes the Kaniadakis logarithm, produces a well-defined thermodynamic framework with a single deformation parameter K and smoothly reduces to the Boltzmann-Gibbs entropy in the limit $K \rightarrow 0$. This property makes the Kaniadakis formalism particularly attractive for gravitational systems, where high-energy corrections and non-Gaussian statistics naturally arise. As shown in [17], the Kaniadakis entropy may be applied to black holes and cosmological horizons by assuming that the horizon microstates follow a κ -deformed statistical distribution. In this case, the entropy becomes a function of the Bekenstein-Hawking entropy given by $S_h = A/4$, where A is the apparent horizon area. Then,

$$S_K(A) = \frac{1}{K} \sinh(K S_h), \quad (2)$$

For small deformations ($K S_h \ll 1$), Eq. (2) expands to

$$S_K(S_h) = S_h + \frac{1}{6} K^2 S_h^3 + \mathcal{O}(K^4), \quad (3)$$

which clearly shows that the leading term reproduces the Bekenstein-Hawking entropy [9, 10]. This unveils that the Kaniadakis modification contributes higher-order geometric corrections to the standard area law. In holographic dark energy models, the energy density is directly linked to the entropy associated with the infrared cutoff length L [30, 31]. In the context of horizon thermodynamics, a modified entropy immediately implies a modified energy associated with the apparent horizon. Using the holographic dark energy argument [30–32], that is,

$$\rho_{de} L^4 \leq S_h, \quad (4)$$

and using the expansion (3) evaluated at the apparent horizon area A , one arrives at

$$\rho_{de} L^4 \leq \frac{A}{4} + \frac{1}{6} K^2 \left(\frac{A}{4}\right)^3, \quad \text{with} \quad \frac{A}{4} = \pi L^2, \quad (5)$$

then

$$\rho_{de} L^4 \leq \pi L^2 + \frac{\pi^3}{6} K^2 L^6 \implies \rho_{de} \leq \pi L^{-2} + \frac{\pi^3}{6} K^2 L^2. \quad (6)$$

Now, considering $L = H^{-1}$, one obtains the HDE model

$$\rho_{\text{de}} = 3c^2 H^2 + \frac{K^2}{H^2}. \quad (7)$$

The expression in Eq. (7) reveals in a transparent way how the Kaniadakis deformation parameter K modifies the standard holographic dark energy prescription. In particular, while the usual term $\rho_{\text{de}} \sim H^2$ arises from the leading Bekenstein–Hawking entropy contribution, the additional term proportional to $K^2 H^{-2}$ originates from the higher-order correction in the entropy expansion. This correction effectively introduces an infrared contribution to the energy density, which becomes dominant in the late-time regime where $H \rightarrow 0$. As a consequence, the Kaniadakis parameter induces a natural self-accelerating behavior without the need of an explicit cosmological constant. From a physical perspective, this shows that the deformation of the entropy-area law propagates non-trivially into the cosmological dynamics, generating a two-scale structure in ρ_{de} : a UV-like term controlled by H^2 and an IR-like term controlled by H^{-2} .

III. THE APPARENT HORIZON DYNAMICS

Let's start by considering a spatially flat ($k = 0$) FLRW Universe,

$$ds^2 = -dt^2 + a^2(t) [dr^2 + r^2 d\Omega^2], \quad (8)$$

where $a(t)$ is the scale factor and $d\Omega^2 = d\theta^2 + \sin^2 \theta d\varphi^2$. For the above line element, the Friedmann field equations read

$$3H^2 = \rho + \rho_{\text{de}}, \quad (9)$$

$$\dot{H} = -\frac{1}{2}(\rho + p + \rho_{\text{de}} + p_{\text{de}}), \quad (10)$$

along with the conservation equations

$$\dot{\rho} + 3H(\rho + p) = 0, \quad \dot{\rho}_{\text{de}} + 3H(\rho_{\text{de}} + p_{\text{de}}) = 0, \quad (11)$$

with Hubble given as usual by $H = \dot{a}/a$. It is worth mentioning that, the components of the Universe for the present case are a perfect fluid matter distribution characterized by $\{\rho, p\}$ and the dark sector described by $\{\rho_{\text{de}}, p_{\text{de}}\}$. Moreover, each sector is separately conserved, meaning that there is not energy exchange between them.

A spatially flat, $k = 0$, FLRW Universe has as causal boundary an apparent horizon R_A coinciding with the Hubble's horizon [33], that is,

$$R_A = \frac{1}{H}, \quad (12)$$

The apparent horizon R_A is the surface satisfying the following equation

$$h^{ij} \nabla_i R \nabla_j R \Big|_{R=R_A} = 0, \quad i, j = t, r, \quad (13)$$

where R is the areal radius defined as $R(t, r) = a(t)r$, being r the co-moving radial distance and h^{ij} the inverse metric of the two-dimensional metric h_{ij} on the t - r plane. These definitions come from the FLRW line element re-expressed using the warped product as [33]

$$ds^2 = h_{ij} dx^i dx^j + R^2 d\Omega^2. \quad (14)$$

As we are going to explore the thermodynamics behavior of this corrected holographic dark energy model, to do so one needs to ensure that all geometric properties can be properly interpreted as thermodynamic variable states. In this regards, to perform a thermodynamics study on the apparent horizon it is necessary to introduce a suitable definition for the surface gravity. Since the apparent horizon is a dynamical object, the surface gravity leading to a temperature definition in this case is the well-known Hayward-Kodama surface gravity given by [34, 35]

$$\kappa = \frac{1}{2\sqrt{-h}} \partial_i (\sqrt{-h} h^{ij} \partial_j R), \quad (15)$$

yielding

$$\kappa = -\frac{R}{2} (\dot{H} + 2H^2). \quad (16)$$

With this expression, one can obtain the temperature at the apparent horizon $R = R_A$ as follows

$$T_A = -\frac{\kappa}{2\pi} = \frac{H}{2\pi} \left(1 - \frac{\dot{R}_A}{2HR_A} \right). \quad (17)$$

The minus sign in front the surface gravity, ensure a positive temperature. This is consistent with the fact that the apparent horizon corresponds to an inner-past horizon, since $\kappa < 0$ [36].

IV. MODIFIED HOLOGRAPHIC DARK ENERGY MODEL AND THE EQUATION OF STATE

Following the approach given in [37], the Friedmann Eq. (9) adopts the following form

$$3H^2 = (1 + r) \left(3c^2 H^2 + \frac{K^2}{H^2} \right). \quad (18)$$

Here, r is the so-called coincident parameter defined by $r \equiv \rho/\rho_{\text{de}}$. The introduction of this parameter is helpful because through it one can check the impact introduced by the dark sector into the thermodynamic description. Now using Eq. (12), the expression (9) can be recast as

$$1 + r = \frac{1}{c^2 + \frac{K^2}{3} R_A^4}. \quad (19)$$

The dynamical nature of the R_A suggests that the thermodynamic first law should be extended as proposed in

[35]. The main ingredients of this formulation are: i) the Misner–Sharp energy, ii) the Hayward-Kodama surface gravity and iii) the areal volume $V_A = \frac{4\pi}{3}R_A^3$. Additionally, it is necessary to introduce new quantities to reach the desired thermodynamics description. These quantities are: iv) the work density W and the v) energy–flux ψ_i across R_A . The definition of these new pieces is given by

$$W \equiv -\frac{1}{2}h_{ij}T^{ij}, \quad (20)$$

and

$$\psi_i \equiv T_i^j \nabla_j R + W \nabla_i R, \quad (21)$$

respectively. Furthermore, T^{ij} represents the projected energy-momentum tensor components and $A\psi_i$ is so-called the energy-supply vector.

Importantly, the work density is related with the pressure of the system. Concretely,

$$P(R_A, T) \equiv W = \frac{1}{2}(\rho - p), \quad (22)$$

where the radius of the R_A is connected with the the specific volume as follows $v = 2R_A$ [38]. Providing, in this way a relation of the type

$$P = P(v, T), \quad (23)$$

as usual. Putting together Eqs. (10), (12), (17), (19) and (22) one gets

$$P = \frac{T_A}{v} + \frac{1}{2} \left[\frac{K^2}{4} v^2 - \frac{12(1/3 - c^2)}{v^2} \right]. \quad (24)$$

It is clear that from (24) that $\{K, c\} = \{0, 0\}$ leads to well-known result for pure Einstein gravity.

Another interesting proposal within the framework of holographic dark energy models, is the Granda-Oliveros (GO) proposal [39]. This provides a causal and fully local reformulation of holographic dark energy by replacing the traditional infrared cutoff-typically associated with the future event horizon with a scale constructed solely from the Hubble parameter and its time derivative.

With this motivation at hand, we propose here the following holographic dark energy model, including both Kaniadakis and GO like contributions

$$\rho_{\text{de}} = 3c^2 H^2 + \frac{K^2}{H^2} + 3\beta \dot{H}. \quad (25)$$

Following a similar procedure, the equation of state (23), in this case, leads to

$$P(v, T) = \left[1 + \frac{3}{2}\beta \right] \frac{T_A}{v} + \frac{1}{2} \left[\frac{K^2}{4} v^2 - \frac{12(1/3 - c^2 + 2\beta)}{v^2} \right]. \quad (26)$$

It is worth mentioning that, to obtain the above expression, the Friedmann equations (9) and (10) took into

account the dynamical contribution given by GO like term.

Now, we are in position to examine the thermodynamics of both models, (24) and (26). This will be matter of the next section.

V. PHASE TRANSITIONS AND CRITICALITY

To study phase transitions, it is important to determine the possible existence of critical points. To do this, one appeals to the critical conditions given by

$$\left(\frac{\partial P}{\partial v} \right) \Big|_{T_A} = \left(\frac{\partial^2 P}{\partial v^2} \right) \Big|_{T_A} = 0. \quad (27)$$

The solution of the above system leads to the critical volume and critical temperature. For the equation of state (24) one obtains

$$v_c = 2 \left(\frac{1/3 - c^2}{K^2} \right)^{1/4}, \quad (28)$$

and

$$T_c = 8(1/3 - c^2) \left(\frac{K^2}{1/3 - c^2} \right)^{1/4}. \quad (29)$$

A positive defined critical volume v_c and critical temperature T_c is possible if and only if the holographic parameter c satisfies $c^2 < \frac{1}{3}$. Besides, the critical pressure is given by

$$P_c = 3\sqrt{1/3 - c^2}K, \quad (30)$$

where the condition imposed on c yields to a real critical pressure. For this system the compressibility factor Z_c is

$$Z_c \equiv \frac{P_c v_c}{T_c} = 2\frac{3}{8}, \quad (31)$$

that is, twice of the given for a genuine Van der Waals liquid-gas phase transition. On the other hand, when β terms are present, from the equation of state (26) the criticality conditions provide the following critical values,

$$v_c = 2 \left(\frac{1/3 - c^2 + 2\beta}{K^2} \right)^{1/4}, \quad (32)$$

and

$$T_c = 8\sqrt{K} (1/3 - c^2 + 2\beta)^{3/4} \left(1 + \frac{3}{2}\beta \right)^{-1}, \quad (33)$$

and

$$P_c = 3\sqrt{1/3 - c^2 + 2\beta}K. \quad (34)$$

Here, Z_c is more involved than in the previous case depending, on the β parameter, that is,

$$\frac{P_c v_c}{T_c} = 2 \left(1 + \frac{3}{2} \beta \right) \frac{3}{8}. \quad (35)$$

Now we are in position to explore the behavior of both, (24) and (26). For the former, in Fig. 1 it is displayed the trend of the pressure against the volume. As can be observed, the model presents an unusual behavior, that is, the phase transition takes place for values of T above the critical one (see blue line). Furthermore, the system starts taking small negative values for the pressure with small volumes and then grows with increasing volume up to a local maximum. This behavior is associated with unstable thermodynamic states, as the isothermal compressibility becomes negative. After reaching the local maximum, the pressure decreases with increasing volume. Here, the system presents an allowed stable thermodynamic state. Nevertheless, at some point the pressure again starts to increase in magnitude with increasing volume. This fact reveals that the system becomes unstable for volumes that are large enough.

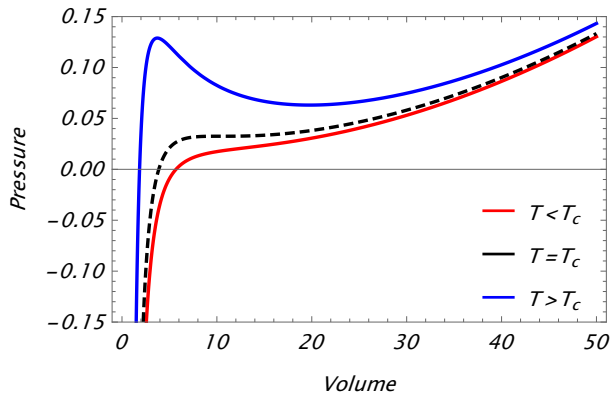


FIG. 1: The trend of the pressure (24) versus the volume for the model (7). The system presents an inverted first order phase transition above the critical temperature. This plot considers $\{c, K\} = \{0.2; 0.02\}$.

To further corroborate the above statements, in Fig. 2 the trend of Gibbs free energy

$$G(v, T) = \frac{4(3c^2 - 1)}{v} + \frac{v^3}{12} K^2 - T \ln v, \quad (36)$$

is depicted. The right panel of Fig. 2 shows a zoom of the Gibbs free energy for $T > T_c$, where the system shows the shape of the swallowtail. In this case, we have an *inverted* swallowtail or a non-physical swallowtail. This is so because the Gibbs free energy is not reaching its minimum value. In comparison with the usual first order phase transition presented by a real gas, here the usual unstable states are not forbidden for the system.

Next, we analyze the case for the equation of state (26). In this case, one can obtain a relation between c and β .

Of course, for $\beta = 0$ one recovers the previous model (24). Besides, as in this model c^2 should be less than unity, we can restrict β considering this fact to have a positive critical volume and critical temperature. Therefore, one has $\beta > (3c^2 - 1)/6$. On the other hand, to further ensure $T_c > 0$ it is necessary to enforce $\beta > -2/3$. If we restrict ourselves to the case $1/3 < c^2 < 1$, then from β 's constraints, the second one can be discarded. The Fig. 3 displays the pressure including the β terms. It can be appreciated that there is an *inverted* first order phase transition.

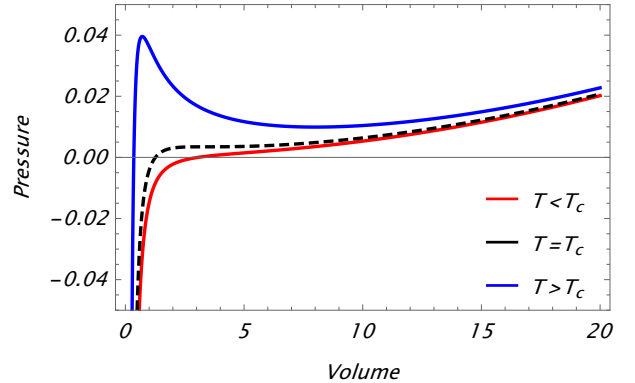


FIG. 3: The trend of the pressure (26) versus the volume for the model (25). The system presents an inverted first order phase transition above the critical temperature. This plot considers $\{c; K; \beta\} = \{0.6; 0.02; 0.015\}$.

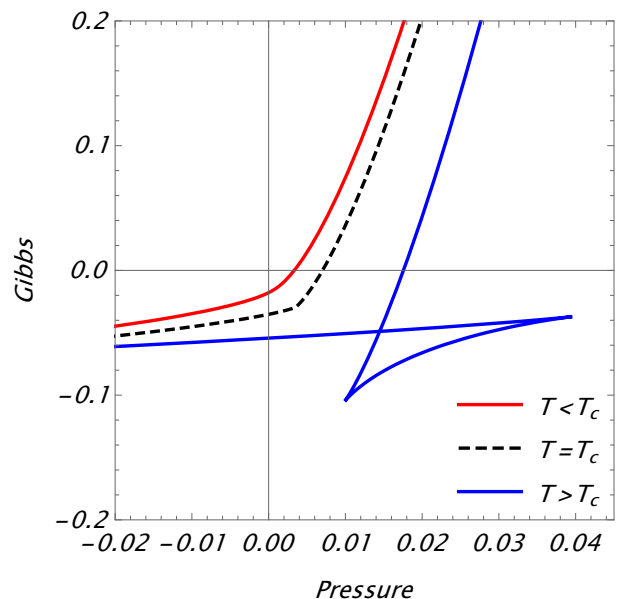


FIG. 4: The Gibbs free energy against the pressure for the model (7). For those values below the critical temperature (red line), the Gibbs function is smooth, while increasing the temperature and crossing the critical one (blue line), appear a non-physical swallowtail shape accounting for a non-conventional first order phase transition.

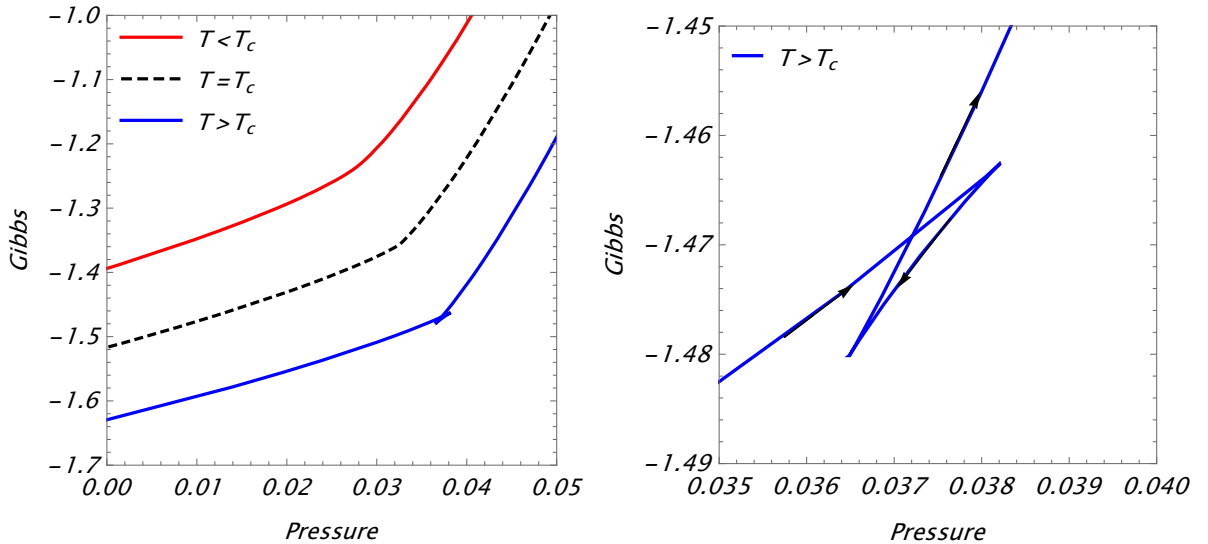


FIG. 2: **Left panel:** The Gibbs free energy against the pressure for the model (25). For those values below the critical temperature (red line), the Gibbs function is smooth, while increasing the temperature and crossing the critical one (blue line), appear a non-physical swallowtail shape accounting for a non-conventional first order phase transition. **Right panel:** A zoom of the swallowtail. It should be taking into account that the curve traversed from small to huge volumes. As the pressure increases with volume, the Gibbs free energy never reaches a minimum value as desired for thermodynamic stability.

For this case, Fig. 4 shows the Gibbs free energy as a function of pressure.

$$G(v, T) = \frac{1}{v} \left[-4 + 12c^2 + k^2 v^4 / 12 - 24\beta - (Tv/2)(2 + 3\beta) \ln v \right]. \quad (37)$$

As before, above the critical temperature the system presents a swallowtail shape which is non-physical.

VI. CLASSICAL STABILITY

To better understand the role played by the parameters c , K and β , we here analyze the minimum criterion to have a stable model. This is based on the sound speed of the content of the matter. As the byrionic matter distribution So, as usual, the sound speed is defined by

$$v_s^2 = \frac{d\rho_{de}}{\rho_{de}} = \frac{d(\omega_{de}\rho_{de})}{d\rho_{de}} = \omega_{de} + \rho_{de} \frac{d\omega_{de}}{d\rho_{de}}. \quad (38)$$

Now, taking into account ρ_{de} given by the expression (7) and the conservation Eq. (11), one obtains

$$1 + \omega_{de} = \frac{2}{3} (1 + q) \left(\frac{3c^2 H^2 - K^2 / H^2}{\rho_{de}} \right). \quad (39)$$

On the other hand, by combining the Friedmann equations, the following result is obtained

$$1 + q = \frac{3}{2} \left(1 + \frac{\omega_{de}\rho_{de}}{\rho + \rho_{de}} \right). \quad (40)$$

Therefore, replacing (40) into (39), one has

$$1 + \omega_{de} = \left(1 + \frac{\omega_{de}\rho_{de}}{\rho + \rho_{de}} \right) \left(\frac{3c^2 H^2 - K^2 / H^2}{\rho_{de}} \right), \quad (41)$$

or in a more compact fashion

$$\omega_{de} = - \left(\frac{1 + r}{1 + r - A} \right) (1 - A), \quad (42)$$

where A is being defined by

$$A = \frac{3c^2 H^2 - K^2 / H^2}{\rho_{de}} = \frac{3c^2 H^2 - K^2 / H^2}{3c^2 H^2 + K^2 / H^2}. \quad (43)$$

In general the expression (43) can be recast as

$$A = 1 - \frac{6K^2}{(1 + r)\rho_{de}^2}, \quad (44)$$

thus, the EoS parameter for the dark (42) sector is given by

$$\omega_{de}(\rho_{de}) = -6K^2 \left[\frac{1 + r}{r(1 + r)\rho_{de}^2 + 6K^2} \right]. \quad (45)$$

Then

$$\frac{d\omega_{de}}{d\rho_{de}} = \omega_{de} \left(\frac{r}{1 + r} \right) \left(\frac{\omega_{de}\rho_{de}}{6K^2} - \frac{1}{\rho_{de}} \right). \quad (46)$$

Returning to Eq. (38) one gets

$$v^2 = \frac{1}{6} \left(\frac{|\omega_{de}|}{K} \right)^2 \left(\rho_{de}^2 - \frac{6K^2}{|\omega_{de}|r} \right) \frac{r}{1+r}. \quad (47)$$

Therefore, stability demands

$$v_s^2 > 0 \implies \rho_{de} > \sqrt{\frac{6}{|\omega_{de}|r}} K. \quad (48)$$

Equation (48) provides a lower bound on the effective dark-energy density required to maintain classical stability whenever v_s^2 is interpreted as a squared effective sound speed. For further details, see Appendices A and B.

VII. MODIFIED FRIEDMANN DYNAMICS AND OBSERVATIONAL CONSTRAINTS

In this section we derive the background cosmological dynamics induced by the Kaniadakis holographic frame-

work, focusing on the explicit form of the Hubble expansion rate $H(z)$, which will later be confronted with observational data through a statistical analysis. We consider a spatially flat FLRW universe filled with a pressureless matter component and an effective dark-energy sector originating from the Kaniadakis entropy of the apparent horizon. The modified Friedmann equation can be written in the standard form

$$3H^2 = \rho_m + \rho_{de}, \quad (49)$$

where ρ_m denotes the matter energy density and ρ_{de} represents the effective Kaniadakis holographic contribution. In the following, we present two particular cases of ρ_{de} and the corresponding expressions for the Hubble function. For further details, see Appendix C.

The first model is defined by expression (7) (Model 1 from now on) and admits an analytic solution for the expansion rate, which can be expressed as

$$H^2(z) = H_0^2 \frac{\Omega_{m0} (1+z)^3 + \sqrt{\Omega_{m0}^2 (1+z)^6 + \frac{2}{3} (1-c^2) \frac{K^2}{H_0^4}}}{2(1-c^2)}, \quad (50)$$

where, $K^2 = 6H_0^4(1-c^2 - \Omega_{m0})$.

For the model given by Eq. (25) (Model 2 from now on), the presence of a term proportional to \dot{H} leads to a first-order differential equation for the Hubble parameter. Rewriting the dynamics in terms of the redshift variable, one obtains

$$\frac{dH}{dz} = \frac{-3(1-c^2)H^2 + 3H_0^2\Omega_{m0}(1+z)^3 + \frac{K^2}{H^2}}{3\beta H(1+z)}. \quad (51)$$

In this case, the expansion history $H(z)$ must be obtained numerically and will be employed in the observational analysis presented in the next section.

VIII. STATISTICAL ANALYSIS: χ^2 ESTIMATORS

In order to constrain the free parameters of the model, we perform a joint likelihood analysis using three independent late-time cosmological probes: Cosmic Chronometers (CC), Type Ia Supernovae (SNe Ia), and Baryon Acoustic Oscillations (BAO) from the DESI DR2 survey. These datasets provide complementary information on the cosmic expansion history and allow us to assess parameter degeneracies in a controlled manner. Assuming

statistical independence among the different probes, the total chi-square function is defined as

$$\chi_{\text{tot}}^2 = \chi_{\text{CC}}^2 + \chi_{\text{SN}}^2 + \chi_{\text{DESI}}^2. \quad (52)$$

In the following, we describe the construction of each individual contribution.

Cosmic Chronometers (CC)

Cosmic chronometers (CC) provide a method to determine the Hubble parameter as a function of redshift in a largely model-independent way. This approach is based on the assumption that the expansion of the Universe causes the ages of passively evolving galaxies to vary with redshift, allowing the expansion rate to be inferred without relying on any cosmological distance ladder. We employ a compilation of N_{CC} measurements $\{z_i, H_{\text{obs}}(z_i), \sigma_{H_i}\}$ from the literature [40–42]. The corresponding chi-square estimator is given by

$$\chi_{\text{CC}}^2 = \sum_{i=1}^{N_{\text{CC}}} \frac{[H_{\text{th}}(z_i; \mathbf{p}) - H_{\text{obs}}(z_i)]^2}{\sigma_{H_i}^2}, \quad (53)$$

where $H_{\text{th}}(z_i; \mathbf{p})$ denotes the theoretical prediction of the Hubble parameter for a given set of model parameters

P.

Type Ia Supernovae (SNe Ia)

Type Ia supernovae provide precise measurements of relative cosmological distances through the distance modulus,

$$\mu_{\text{obs}} = m_B^{\text{corr}} - M, \quad (54)$$

where m_B^{corr} is the corrected apparent magnitude and M denotes the absolute magnitude of the standard candle. The theoretical distance modulus is computed as

$$\mu_{\text{th}}(z; \mathbf{p}) = 5 \log_{10} \left[\frac{D_L(z; \mathbf{p})}{\text{Mpc}} \right] + 25, \quad (55)$$

with the luminosity distance given by

$$D_L(z; \mathbf{p}) = (1+z) \int_0^z \frac{cdz'}{H(z'; \mathbf{p})}. \quad (56)$$

We use the PantheonPlus compilation [43–45]², which contains 1657 SNe Ia with $z > 0.01$. The associated chi-square function is defined as

$$\chi_{\text{SN}}^2 = (\boldsymbol{\mu}_{\text{obs}} - \boldsymbol{\mu}_{\text{th}})^T \mathbf{C}^{-1} (\boldsymbol{\mu}_{\text{obs}} - \boldsymbol{\mu}_{\text{th}}), \quad (57)$$

where \mathbf{C} is the full covariance matrix including both statistical and systematic uncertainties. It is important to note that SNe Ia constrain only relative distances and are therefore insensitive to the absolute expansion scale. As a consequence, the parameters M and H_0 appear in a degenerate combination, which cannot be broken by supernova data alone. In our analysis, this degeneracy is lifted only when SNe Ia are combined with probes that provide absolute measurements of the expansion rate.

Baryon Acoustic Oscillations (DESI)

Baryon acoustic oscillations constitute a robust standard ruler for cosmological distance measurements. We employ the latest BAO data from the DESI DR2 release [46, 47]³, which provide separate measurements of the transverse comoving distance and the Hubble distance. The observational data vector is defined as

$$\mathbf{X}_{\text{obs}} = \left\{ \frac{D_M(z)}{r_d}, \frac{D_H(z)}{r_d}, \frac{D_V(z)}{r_d} \right\}_{\text{obs}}, \quad (58)$$

where $D_M(z) = \int_0^z \frac{c}{H(z')} dz'$ is the transverse comoving distance, $D_H(z) = c/H(z)$ is the Hubble distance, and

$D_V(z) = \left[D_M^2(z) \frac{cz}{H(z)} \right]^{1/3}$ denotes the volume-averaged distance. The theoretical counterpart \mathbf{X}_{th} is constructed analogously. The BAO chi-square is given by

$$\chi_{\text{DESI}}^2 = (\mathbf{X}_{\text{obs}} - \mathbf{X}_{\text{th}})^T \mathbf{C}^{-1} (\mathbf{X}_{\text{obs}} - \mathbf{X}_{\text{th}}), \quad (59)$$

where \mathbf{C} is the covariance matrix provided by the DESI collaboration. Since the model considered in this work is defined only at late times and does not modify the early-Universe physics that determines the sound horizon, we fix the sound horizon at the drag epoch to its Λ CDM value, $r_d = 147.09 \text{ Mpc}$ [48].

A. Model 1

Figure 5 and table I show the background constraints obtained from CC + PantheonPlus + DESI RD2 for three fixed values of the parameter c^2 . While the inferred value of Ω_{m0} shifts systematically as c varies, the posterior distributions of the Hubble constant H_0 and the supernova absolute magnitude M remain unchanged. This behaviour reflects the fact that late-time background observables are sensitive only to a specific combination of Ω_{m0} and c , such that changes in c can be exactly compensated by a rescaling of Ω_{m0} . As a consequence, fixing different values of c leads to different effective matter densities today, without affecting either the expansion history or the quality of the fit to the data. Figure 6 and table II illustrate the complementary situation in which the present-day matter density Ω_{m0} is fixed to different values, while the parameter c is treated as a free variable. In this case, apparently well-defined posterior distributions for c emerge. However, these constraints are entirely driven by the imposed value of Ω_{m0} and do not originate from the data themselves. This behaviour directly reflects the exact degeneracy between Ω_{m0} and c at the background level: once Ω_{m0} is fixed, the value of c is determined, while the expansion history and the agreement with the observational data remain unchanged. Taken together, Figures 5 and 6 demonstrate that late-time background data constrain the expansion history only through a degenerate combination of Ω_{m0} and c . As a result, neither parameter can be independently determined from CC, SN, and BAO data alone. Any apparent constraint on c obtained by fixing Ω_{m0} , or vice versa, is therefore prior-driven and does not represent an observational determination. This motivates the inclusion of perturbation-level observables, which may provide additional sensitivity to the parameter c beyond the homogeneous background expansion.

B. Model 2

Figure 7 and table III present the background constraints obtained from the joint CC + PantheonPlus + DESI

² Available at <https://github.com/PantheonPlusSHOES>.

³ Available at https://github.com/CobayaSampler/bao_data/.

TABLE I: Constraints from CC + PantheonPlus + DESI for different fixed values of c^2 . We report mean values with 68% confidence levels, best-fit values for the free parameters, and the corresponding best-fit value of K/H_0^4 .

Parameter	$c^2 = 0$	$c^2 = 1/6$	$c^2 = 1/3$
<i>Mean values and 68% CL</i>			
H_0	71.83 ± 0.43	71.83 ± 0.44	71.83 ± 0.43
Ω_{m0}	0.318 ± 0.007	0.265 ± 0.006	0.212 ± 0.005
M	-19.337 ± 0.012	-19.337 ± 0.012	-19.336 ± 0.012
<i>Best-fit values</i>			
H_0	71.84	71.88	71.84
Ω_{m0}	0.317	0.264	0.212
M	-19.336	-19.335	-19.336
<i>Derived quantity (best fit)</i>			
K^2/H_0^4	4.10	3.42	2.73

TABLE II: Constraints from CC + PantheonPlus + DESI for different fixed values of Ω_{m0} . We report mean values with 68% confidence levels, best-fit values for the free parameters, and the corresponding best-fit value of K/H_0^4 .

Parameter	$\Omega_{m0} = 0.32$	$\Omega_{m0} = 0.30$	$\Omega_{m0} = 0.28$
<i>Mean values and 68% CL</i>			
H_0	71.86 ± 0.45	71.85 ± 0.43	71.84 ± 0.44
c^2	0.010 ± 0.023	0.054 ± 0.021	0.117 ± 0.020
M	-19.336 ± 0.012	-19.336 ± 0.012	-19.336 ± 0.012
<i>Best-fit values</i>			
H_0	71.85	71.85	71.85
c^2	0.009	0.054	0.117
M	-19.336	-19.336	-19.336
<i>Derived quantity (best fit)</i>			
K^2/H_0^4	4.08	4.18	4.24

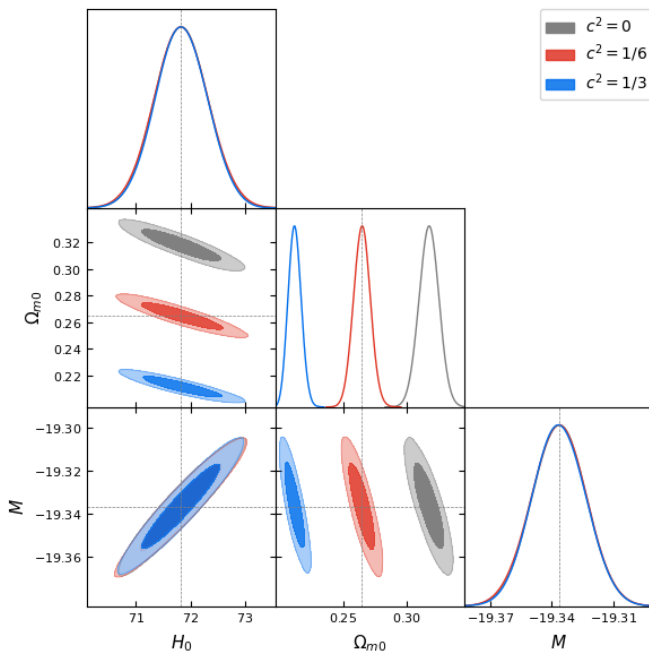


FIG. 5: Triangle plot showing the joint constraints from CC + PantheonPlus + DESI for three fixed values of the parameter c^2 , for model 1, Eq. (50). While the inferred value of the present-day matter density Ω_{m0} shifts systematically as c varies, the posterior distributions of the Hubble constant H_0 and the supernova absolute magnitude M remain unchanged. This behavior reflects the exact degeneracy between Ω_{m0} and c at the background level, indicating that late-time expansion data are insensitive to c .

RD2 analysis for the extended model including the additional parameter β , for three fixed values of the present-day matter density Ω_{m0} . As in Model 1, the posterior distributions of the Hubble constant H_0 and the supernova absolute magnitude M remain remarkably stable under variations of Ω_{m0} , indicating that these quantities

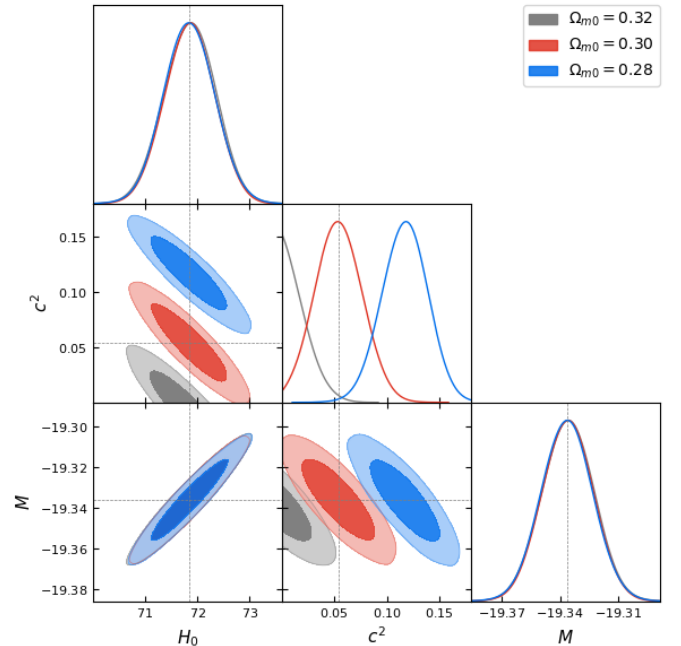


FIG. 6: Triangle plot showing the joint constraints from CC + PantheonPlus + DESI for three fixed values of the present-day matter density Ω_{m0} , for model 1, Eq. (50). In this case, apparently well-defined posterior distributions for the parameter c emerge. However, these constraints are entirely driven by the imposed value of Ω_{m0} and do not originate from the data themselves. This behaviour reflects the exact degeneracy between Ω_{m0} and c at the background level: once Ω_{m0} is fixed, the value of c is algebraically determined, while the expansion history and the quality of the fit remain unchanged.

are robustly determined by late-time background observables.

In contrast, the parameters characterizing differences from the standard cosmology, namely c^2 , K^2/H_0^4 , and β , reveal considerable degeneracies. In particular, vari-

ations in Ω_{m0} are systematically compensated by correlated shifts among these parameters, leading to nearly identical expansion histories and comparable goodness-of-fit to the data. As a result, different combinations of $(c^2, K^2/H_0^4, \beta)$ can reproduce the same late-time background evolution for a fixed value of Ω_{m0} .

This behaviour reflects the fact that, at the background level, the effects of c^2 , K^2/H_0^4 , and β enter the Friedmann equation in a highly correlated manner. Consequently, once Ω_{m0} is fixed, the remaining parameters are effectively constrained along degenerate directions within parameter space, and any apparent bounds on c^2 , K^2/H_0^4 , or β are largely driven by the imposed prior on Ω_{m0} rather than by the observational data themselves.

Taken together, these findings show that including the additional parameter β increases the dimensionality of the parameter space without lifting the intrinsic degeneracies at the background level. Late-time background observables alone are therefore insufficient to independently constrain the parameters $(c^2, K^2/H_0^4, \beta)$. This motivates the inclusion of perturbation-level observables, which may provide additional constraints to these parameters and break the degeneracies identified here.

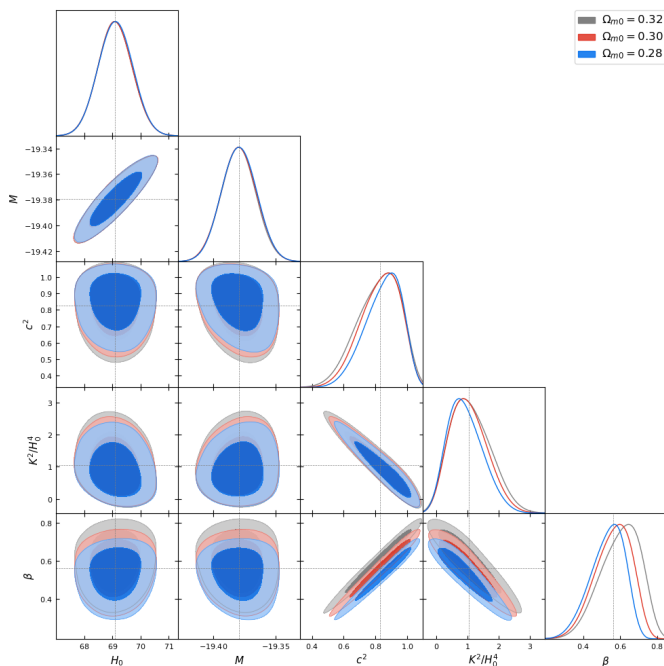


FIG. 7: Posterior distributions and two-dimensional marginalized confidence regions at 68% and 95% CL for model 2, Eq. (51), parameters $(H_0, M, c^2, K^2/H_0^4, \beta)$ obtained from the joint CC+PantheonPlus+DESI analysis. The different colors correspond to fixed values of the matter density parameter $\Omega_{m0} = 0.28$ (blue), 0.30 (red), and 0.32 (gray). While the constraints on H_0 and M remain remarkably stable, the parameters c^2 , K^2/H_0^4 , and β exhibit significant degeneracies, indicating that late-time background observables alone are insufficient to break these correlations.

TABLE III: Constraints from CC + PantheonPlus + DESI for the second model including the parameter β , for different fixed values of the present-day matter density Ω_{m0} . We report mean values with 68% confidence levels and the corresponding best-fit values.

Parameter	$\Omega_{m0} = 0.32$	$\Omega_{m0} = 0.30$	$\Omega_{m0} = 0.28$
<i>Mean values and 68% CL</i>			
H_0	69.10 ± 0.54	69.09 ± 0.55	69.11 ± 0.55
M	-19.380 ± 0.012	-19.379 ± 0.013	-19.379 ± 0.013
c^2	0.819 ± 0.127	0.829 ± 0.124	0.847 ± 0.115
K^2/H_0^4	1.10 ± 0.75	1.04 ± 0.69	0.94 ± 0.66
β	0.600 ± 0.088	0.561 ± 0.081	0.529 ± 0.083
<i>Best-fit values</i>			
H_0	69.09	69.12	69.12
M	-19.381	-19.380	-19.381
c^2	0.899	0.903	0.928
K^2/H_0^4	0.733	0.701	0.549
β	0.662	0.620	0.592

IX. CONCLUDING REMARKS

In this work, we have developed a comprehensive analysis of the cosmological and thermodynamic consequences of a holographic formulation of dark energy based on the Kaniadakis entropic deformation. By incorporating this generalization of the Bekenstein-Hawking entropy within a spatially flat FLRW background, we demonstrate that the dark sector acquires a distinctive infrared correction proportional to H^{-2} , which substantially modifies the dynamics of the apparent horizon and, by extension, the thermodynamic structure of the Universe.

One of the most relevant results of the study is the derivation of an effective dark energy density of the form (7) where the infrared term emerges directly from the structure of the warped entropy and not from an ad hoc geometric choice. This result establishes an explicit connection between relativistic non-extensive statistics and late cosmological dynamics, providing a physically transparent way to introduce modifications to the standard holographic scenario.

From a thermodynamic point of view, the formulation based on the Hayward-Kodama formalism and the unified first law allowed the derivation of a geometric equation of state for the apparent horizon. Criticality analysis reveals the existence of a well-defined critical point and a Van der Waals-type structure; however, the system's behavior exhibits a highly unconventional feature: the appearance of an inverted first-order phase transition at temperatures above the critical temperature. This feature is accompanied by a swallowtail-type structure in the Gibbs free energy that does not reach a thermodynamic minimum, indicating the presence of unstable branches and suggesting limits to the equilibrium interpretation for dynamical cosmological horizons.

Extending the model with a dynamical term proportional to \dot{H} —inspired by the Granda-Oliveros prescription—does not alter the qualitative nature of these phenomena, but it intensifies the deviations from standard thermodynamic behavior. This result is particularly significant, as it indicates that the critical structure is not an artifact of a specific parameterization, but rather a robust consequence of entropic deformation.

The classical stability study allowed us to establish a lower bound for the dark energy density by requiring a positive effective speed of sound. This condition introduces clear physical constraints on the parameter space and strengthens the internal consistency of the model, showing that infrared modification can sustain dynamically stable configurations within a realistic cosmological regime.

From an observational standpoint, the joint statistical analysis using cosmic chronometers, Type Ia supernovae (PantheonPlus), and baryonic acoustic oscillations from DESI demonstrates that the model is compatible with the late expansion history. However, a structural degeneracy is identified between the holographic parameters and the density of matter present, preventing their independent determination at the cosmological background level. This finding has an important implication: expansion data alone are insufficient to discriminate the physics associated with the Kaniadakis deformation, making the incorporation of perturbation observables essential to overcome these degeneracies.

Taken together, the results position Kaniadakis's entropy-based holographic cosmology as a theoretical framework capable of linking gravitational thermodynamics, generalized statistical mechanics, and dark energy dynamics within a coherent structure. Furthermore, the infrared term introduces a late sensitivity absent in other entropic generalizations, potentially offering new insights into the microphysical mechanisms responsible for cosmic acceleration.

Among the main applications of this work are: (i) the study of cosmological perturbations to assess structure formation and break parametric degeneracies, (ii) stability analysis beyond the classical regime, incorporating criteria of causality and scale-dependent perturbations, and (iii) the exploration of non-equilibrium thermodynamic formulations that allow for a deeper interpretation of the nature of the observed inverted transitions.

In summary, this study shows that Kaniadakis entropic deformations not only generate quantitative corrections to the holographic paradigm, but also introduce qualitatively new critical phenomena into horizon thermodynamics. These results open a promising avenue for investigating the relationship between gravitational microstructure and cosmic acceleration, suggesting that the statistical physics underlying the horizon could play a central role in understanding the dark sector of the Universe.

Acknowledgements

M. Gonzalez-Espinoza acknowledges the financial support of FONDECYT de Postdoctorado, N° 3230801. S. Lepe acknowledges the financial support of Fondecyt Grant No.1250969 and J. Saavedra acknowledges the financial support of Fondecyt Grant 1220065.

Appendix A: Cosmological dynamics with generalized holographic dark energy

We consider a generalized holographic dark energy density of the form

$$\rho_{\text{de}} = 3c^2 H^2 + \frac{K^2}{H^2}, \quad (\text{A1})$$

where c^2 and K are constant parameters.

The Friedmann equations for a spatially flat universe ($k = 0$) read

$$3H^2 = \rho + \rho_{\text{de}}, \quad (\text{A2})$$

$$\dot{\rho} + 3H(\rho + p) = 0, \quad \dot{\rho}_{\text{de}} + 3H(\rho_{\text{de}} + p_{\text{de}}) = 0, \quad (\text{A3})$$

$$-2\dot{H} = \rho + p + \rho_{\text{de}} + p_{\text{de}}. \quad (\text{A4})$$

Substituting the expression for ρ_{de} into the Friedmann constraint, we obtain an algebraic equation for $H(z)$,

$$H^2(z) = \frac{1}{6(1-c^2)} \left[1 + \sqrt{1 + \frac{12(1-c^2)K^2}{\rho^2(z)}} \right] \rho(z). \quad (\text{A5})$$

An interesting feature of this model is the existence of a self-accelerating solution even in the absence of standard matter, i.e., for $\rho \rightarrow 0$, provided that $c^2 < 1$. In this limit, the Hubble parameter approaches a constant value,

$$H = \left(\frac{3}{1-c^2} \right)^{1/4} \sqrt{\frac{K}{3}}. \quad (\text{A6})$$

Assuming a barotropic equation of state $p = \omega\rho$ with constant ω , the matter density evolves as

$$\rho(z) = \rho_0(1+z)^{3(1+\omega)}. \quad (\text{A7})$$

For $\omega > -1$, one has $\rho(z \rightarrow -1) \rightarrow 0$, and therefore

$$H(z \rightarrow -1) \rightarrow \left(\frac{3}{1-c^2} \right)^{1/4} \sqrt{\frac{K}{3}}. \quad (\text{A8})$$

This asymptotic behavior resembles that of the Λ CDM model,

$$3H^2(z) = \rho_0(1+z)^3 + \Lambda, \quad (\text{A9})$$

for which $H(z \rightarrow -1) \rightarrow \sqrt{\Lambda/3}$. This suggests the identification

$$K = \sqrt{\frac{1-c^2}{3}} \Lambda, \quad (\text{A10})$$

which provides an effective interpretation of the parameter K in terms of a cosmological constant.

a. Deceleration parameter. Using the Friedmann equations, the deceleration parameter is given by

$$q = -1 + \frac{3}{2} \left(1 + \frac{p + p_{\text{de}}}{\rho + \rho_{\text{de}}} \right) = \frac{1}{2} [1 + 3(\omega\Omega + \omega_{\text{de}}\Omega_{\text{de}})], \quad (\text{A11})$$

where we have introduced the density parameters

$$\Omega = \frac{\rho}{3H^2}, \quad \Omega_{\text{de}} = \frac{\rho_{\text{de}}}{3H^2} = c^2 + \frac{K^2}{3H^4}. \quad (\text{A12})$$

From the above expression, one obtains

$$\omega\Omega + \omega_{\text{de}}\Omega_{\text{de}} = \frac{1}{3}(2q - 1). \quad (\text{A13})$$

In the case of cold dark matter ($\omega = 0$), the deceleration parameter constrains the dark energy equation of state. In particular:

- For quintessence ($-1 < \omega_{\text{de}} < -1/3$),

$$-\frac{1}{2}(3\Omega_{\text{de}} + 1) < q < \frac{1}{2}(1 - \Omega_{\text{de}}). \quad (\text{A14})$$

- For phantom dark energy ($\omega_{\text{de}} < -1$),

$$q < -\frac{1}{2}(3\Omega_{\text{de}} - 1). \quad (\text{A15})$$

These relations may provide observational insight into the present value of Ω_{de} , which in this model reads

$$\Omega_{\text{de}}(0) = c^2 + \frac{K^2}{3H_0^4}. \quad (\text{A16})$$

This raises the question of whether observations can independently constrain both parameters c^2 and K .

b. Including \dot{H} corrections. A natural extension of the model consists in adding a term proportional to \dot{H} in the dark energy density,

$$\rho_{\text{de}} = 3c^2 H^2 + \frac{K^2}{H^2} + 3\beta\dot{H}, \quad (\text{A17})$$

where β is a constant parameter.

Substituting this expression into the Friedmann constraint leads to the differential equation

$$\frac{dH^2}{dz} + \frac{2}{\beta}(1 - c^2) \frac{H^2}{1+z} = \frac{2}{3\beta} \left(\rho + \frac{K^2}{H^2} \right) \frac{1}{1+z}, \quad (\text{A18})$$

where we have used the relation

$$\dot{H} = -\frac{1}{2}(1+z) \frac{dH^2}{dz}. \quad (\text{A19})$$

Appendix B: Effective Dark-Energy Equation of State and Regimes

The effective dark-energy equation-of-state parameter can be written in the form

$$\omega_{\text{de}} = -1 + (1 + \omega) \frac{Ar}{1 + r - A}, \quad (\text{B1})$$

where the auxiliary quantity A is defined as

$$A = \frac{3c^2 H^2 - K^2/H^2}{3c^2 H^2 + K^2/H^2}. \quad (\text{B2})$$

Here r denotes the ratio of energy densities (as defined in the main text), and ω is the equation-of-state parameter of the matter sector.

Sign of A and corresponding dynamical regimes

From Eq. (B2) it follows that

$$0 < A < 1 \quad \rightarrow \quad H^2 > \frac{1}{\sqrt{3}c} K, \quad (\text{B3})$$

$$A < 0 \quad \rightarrow \quad H^2 < \frac{1}{\sqrt{3}c} K. \quad (\text{B4})$$

If the condition (B4) holds ($A < 0$), then Eq. (B1) becomes

$$\omega_{\text{de}} = -1 - (1 + \omega) \frac{|A|r}{1 + r + |A|} \quad (\text{phantom regime}). \quad (\text{B5})$$

If instead (B3) holds ($0 < A < 1$), then ω_{de} may lie in a quintessence-like range,

$$-1 < \omega_{\text{de}} < -\frac{1}{3} \quad \rightarrow \quad 0 < (1 + \omega) \frac{Ar}{1 + r - A} < \frac{2}{3}, \quad (\text{B6})$$

or it may satisfy

$$\omega_{\text{de}} > 0 \quad \rightarrow \quad (1 + \omega) \frac{Ar}{1 + r - A} > 1. \quad (\text{B7})$$

From the standpoint of interpreting ρ_{de} as an effective dark-energy component driving cosmic acceleration, the case (B7) (i.e. $\omega_{\text{de}} > 0$) is typically regarded as physically implausible for late-time acceleration. Therefore, the phenomenologically relevant regimes are usually those described by either the phantom condition (B5) or the quintessence-like condition (B6).

Appendix C: The Case $\beta = 0$ and Explicit Expressions for $q(z)$ and $T_A(z)$

Setting $\beta = 0$, the Hubble function simplifies to

$$H^2(z) = \frac{H_0^2}{2(1-c^2)} \left[\Omega(z) + \sqrt{\Omega^2(z) + \frac{4(1-c^2)K^2}{3H_0^2}} \right]. \quad (\text{C1})$$

For cold dark matter ($\omega = 0$), one has $\Omega(z) = \Omega_0(1+z)^3$, and Eq. (C1) becomes

$$H^2(z) = \frac{H_0^2}{2(1-c^2)} \left[\Omega_0(1+z)^3 + \sqrt{\Omega_0^2(1+z)^6 + \frac{4(1-c^2)K^2}{3H_0^2}} \right]. \quad (\text{C2})$$

Apparent-horizon temperature

The apparent-horizon temperature can be expressed as

$$T_A(z) = \frac{H(z)}{4\pi} [1 - q(z)], \quad q = -1 \rightarrow T_A(z) = \frac{H(z)}{2\pi}. \quad (\text{C3})$$

Thus, when the background approaches a de Sitter stage ($q \rightarrow -1$), the temperature reduces to the Kodama-Hayward form shown in Eq. (C3).

From time derivatives to redshift derivatives

Using $dz/dt = -(1+z)H$, one may rewrite \dot{H} in terms of derivatives with respect to z as

$$\dot{H} = -\frac{1}{2}(1+z) \frac{dH^2}{dz}. \quad (\text{C4})$$

Since the deceleration parameter is $q = -1 - \dot{H}/H^2$, this becomes

$$q(z) = -1 + \frac{1}{2}(1+z) \frac{1}{H^2} \frac{dH^2}{dz}. \quad (\text{C5})$$

Differentiating Eq. (C2) with respect to z yields

$$\frac{dH^2}{dz} = \frac{3H_0^2\Omega_0}{2(1-c^2)} \left(1 + \frac{\Omega_0(1+z)^3}{\sqrt{\Omega_0^2(1+z)^6 + 4(1-c^2)K^2/(3H_0^2)}} \right) (1+z)^2. \quad (\text{C6})$$

Substituting Eq. (C6) into Eq. (C5), one obtains the explicit deceleration parameter

$$q(z) = -1 + \frac{3}{2} \left(\frac{\Omega_0(1+z)^3}{\sqrt{\Omega_0^2(1+z)^6 + 4(1-c^2)K^2/(3H_0^2)}} \right). \quad (\text{C7})$$

From Eq. (C7) it follows immediately that

$$q(z \gg 0) \sim \frac{1}{2}, \quad q(z \rightarrow -1) \rightarrow -1, \quad (\text{C8})$$

corresponding to an early-time matter-dominated regime ($q = 1/2$) and a late-time cosmological-constant-like regime ($q \rightarrow -1$).

Early- and late-time limits of $H(z)$ and $T_A(z)$

From Eq. (C2) one finds

$$H(z \gg 0) \sim H_0 \sqrt{\frac{\Omega_0}{1-c^2}} (1+z)^3, \quad H(z \rightarrow -1) \rightarrow \sqrt{\frac{H_0 K}{\sqrt{3(1-c^2)}}}, \quad (\text{C9})$$

and the late-time limit in Eq. (C9) coincides with the limit found in Eq. (A8).

Using Eq. (C3), the temperature behaves as

$$T_A(z \gg 0) \sim \frac{H_0}{8\pi} \sqrt{\frac{\Omega_0}{1-c^2}} (1+z)^3, \quad T_A(z \rightarrow -1) \rightarrow \frac{1}{2\pi} \sqrt{\frac{H_0 K}{\sqrt{3}(1-c^2)}}. \quad (\text{C10})$$

Present-day constraint and parameter estimates

Evaluating Eq. (C7) at $z = 0$ gives

$$q(0) = -1 + \frac{3}{2} \left(\frac{\Omega_0}{\sqrt{\Omega_0^2 + 4(1-c^2)K^2/(3H_0^2)}} \right). \quad (\text{C11})$$

As a simple estimate, if one adopts $q(0) \simeq -0.55$ and

$\Omega_0 \simeq 0.3$, then $q(0) \simeq -1/2$ suggests a solution

$$\frac{K}{H_0} \sim \sqrt{\frac{6}{1-c^2}} \Omega_0, \quad (\text{C12})$$

which still contains two unknowns, c^2 and K .

From Eq. (A5) with $\beta = 0$, one obtains at $z = 0$ the exact relation

$$1 = \frac{\Omega_0}{2(1-c^2)} \left[1 + \sqrt{1 + \frac{4(1-c^2)K^2}{3H_0^2\Omega_0^2}} \right] \implies \frac{K}{H_0} = \sqrt{3[1-c^2-\Omega_0]}. \quad (\text{C13})$$

Combining Eqs. (C12) and (C13) yields

$$\sqrt{\frac{6}{1-c^2}} \Omega_0 \sim \sqrt{3[1-c^2-\Omega_0]}, \quad (\text{C14})$$

which implies

$$\left(\frac{2\Omega_0}{1-c^2} + 1 \right) \Omega_0 \sim 1 - c^2 \implies c^2 \sim 1 - 2\Omega_0. \quad (\text{C15})$$

Substituting Eq. (C15) into Eq. (C13) then gives

$$K \sim \sqrt{3\Omega_0} H_0. \quad (\text{C16})$$

Therefore, one arrives at the rough estimates

$$c^2 \sim 1 - 2\Omega_0, \quad K \sim \sqrt{3\Omega_0} H_0, \quad (\text{C17})$$

showing explicitly how observations of Ω_0 and H_0 could be used to infer (c^2, K) at the level of order-of-magnitude estimates.

Finally, if one compares the late-time limit in Eq. (C9) with the Λ CDM expectation $H(z \rightarrow -1) \rightarrow \sqrt{\Lambda/3}$, one obtains

$$H(z \rightarrow -1) \rightarrow \sqrt{\frac{H_0 K}{\sqrt{3}(1-c^2)}} \sim \sqrt{\frac{\Lambda}{3}}, \quad (\text{C18})$$

which suggests the scaling

$$H_0 K \sim \sqrt{\frac{1}{3}(1-c^2)} \Lambda, \quad (\text{C19})$$

and using Eq. (C15) this may be expressed as

$$K \sim \sqrt{\frac{2\Omega_0}{3}} \frac{\Lambda}{H_0}. \quad (\text{C20})$$

[1] P. Collaboration, Planck 2018 results. vi. cosmological parameters, *Astronomy & Astrophysics* 641 (2020) A6. [arXiv:1807.06209](https://arxiv.org/abs/1807.06209).

[2] S. Alam, et al., The SDSS-IV extended Baryon Oscilla-

tion Spectroscopic Survey (eBOSS): final measurement of $H(z)$ from the baryon acoustic oscillation measurements between redshifts 0.6 and 3.5, *Monthly Notices of the Royal Astronomical Society* 506 (1) (2021) 951–975.

- arXiv:2007.08991, doi:10.1093/mnras/stab1811.
- [3] A. G. Riess, et al., A comprehensive measurement of the local value of the hubble constant with 1 km/s/mpc uncertainty from the hubble space telescope and the sh0es team, *The Astrophysical Journal Letters* 934 (1) (2022) L7. arXiv:2112.04510, doi:10.3847/2041-8213/ac5c5b.
 - [4] S. Weinberg, The cosmological constant problem, *Reviews of Modern Physics* 61 (1989) 1–23.
 - [5] I. Zlatev, L. Wang, P. J. Steinhardt, Quintessence, cosmic coincidence, and the cosmological constant, *Physical Review Letters* 82 (1999) 896. arXiv:astro-ph/9807002.
 - [6] M. Li, A model of holographic dark energy, *Physics Letters B* 603 (2004) 1. arXiv:hep-th/0403127.
 - [7] G. 't Hooft, Dimensional reduction in quantum gravity, *Salamfestschrift* (1993). arXiv:gr-qc/9310026.
 - [8] L. Susskind, The world as a hologram, *Journal of Mathematical Physics* 36 (1995) 6377. arXiv:hep-th/9409089.
 - [9] J. D. Bekenstein, Black holes and entropy, *Phys. Rev. D* 7 (1973) 2333–2346. doi:10.1103/PhysRevD.7.2333.
 - [10] S. W. Hawking, Particle creation by black holes, *Commun. Math. Phys.* 43 (1975) 199–220. doi:10.1007/BF02345020.
 - [11] C. Tsallis, Possible generalization of boltzmann–gibbs statistics, *Journal of Statistical Physics* 52 (1988) 479.
 - [12] A. Rényi, On measures of entropy and information, *Proceedings of the Fourth Berkeley Symposium* (1961).
 - [13] J. D. Barrow, The area of a rough black hole, *Physics Letters B* 808 (2020) 135643.
 - [14] G. Kaniadakis, Non-linear kinetics underlying generalized statistics, *Physica A* 296 (2001) 405–425. doi:10.1016/S0378-4371(01)00184-4.
 - [15] G. Kaniadakis, Statistical mechanics in the context of special relativity, *Phys. Rev. E* 66 (2002) 056125. doi:10.1103/PhysRevE.66.056125.
 - [16] N. Drepanou, A. Lymperis, E. N. Saridakis, K. Yesmakhanova, Kaniadakis holographic dark energy and cosmology, *European Physical Journal C* 82 (2022) 449. arXiv:2109.09181.
 - [17] H. Moradpour, A. Ziaie, M. K. Zangeneh, Generalized entropies and corresponding holographic dark energy models, *European Physical Journal C* 80 (2020) 732. arXiv:2005.06271.
 - [18] H. Kodama, Conserved energy flux for the spherically symmetric system, *Progress of Theoretical Physics* 63 (1980) 1217.
 - [19] S. A. Hayward, Unified first law of black hole dynamics and relativistic thermodynamics, *Classical and Quantum Gravity* 15 (1998) 3147.
 - [20] C. W. Misner, D. H. Sharp, Relativistic equations for adiabatic, spherically symmetric gravitational collapse, *Physical Review* 136 (1964) B571.
 - [21] T. Jacobson, Thermodynamics of space-time: The Einstein equation of state, *Phys. Rev. Lett.* 75 (1995) 1260–1263. arXiv:gr-qc/9504004, doi:10.1103/PhysRevLett.75.1260.
 - [22] M. e. a. Moresco, A 6% measurement of the hubble parameter at $z = 0.45$: direct evidence of the epoch of cosmic re-acceleration, *JCAP* 05 (2016) 014.
 - [23] A. L. e. a. Ratsimbazafy, Age-dating luminous red galaxies observed with the southern african large telescope, *MNRAS* 467 (2017) 3239.
 - [24] D. e. a. Brout, The pantheon+ analysis: Cosmological constraints, *ApJ* 938 (2022) 110.
 - [25] A. G. e. a. Adame, DESI 2024 VI: cosmological constraints from the measurements of baryon acoustic oscillations, *JCAP* 02 (2025) 021. arXiv:2404.03002, doi:10.1088/1475-7516/2025/02/021.
 - [26] M. A.-K. et al., DESI DR2 results. II. Measurements of baryon acoustic oscillations and cosmological constraints, *Phys. Rev. D* 112 (2025) 083515. arXiv:2503.14738, doi:10.1103/tr6y-kpc6.
 - [27] E. V. Linder, Cosmic growth history and expansion history, *Phys. Rev. D* 72 (2005) 043529.
 - [28] Y. Wang, Figure of merit for dark energy constraints from current observational data, *Phys. Rev. D* 77 (2008) 123525.
 - [29] L. Granda, A. Oliveros, Infrared cut-off proposal for the holographic density, *Physics Letters B* 669 (2008) 275. arXiv:0810.3149.
 - [30] M. Li, A Model of holographic dark energy, *Phys. Lett. B* 603 (2004) 1. arXiv:hep-th/0403127, doi:10.1016/j.physletb.2004.10.014.
 - [31] S. Wang, Y. Wang, M. Li, Holographic Dark Energy, *Phys. Rept.* 696 (2017) 1–57. arXiv:1612.00345, doi:10.1016/j.physrep.2017.06.003.
 - [32] H. Moradpour, A. H. Ziaie, M. Kord Zangeneh, Generalized entropies and corresponding holographic dark energy models, *Eur. Phys. J. C* 80 (8) (2020) 732. arXiv:2005.06271, doi:10.1140/epjc/s10052-020-8307-x.
 - [33] V. Faraoni, Cosmological apparent and trapping horizons, *Phys. Rev. D* 84 (2011) 024003. arXiv:1106.4427, doi:10.1103/PhysRevD.84.024003.
 - [34] H. Kodama, Conserved Energy Flux for the Spherically Symmetric System and the Back Reaction Problem in the Black Hole Evaporation, *Prog. Theor. Phys.* 63 (1980) 1217. doi:10.1143/PTP.63.1217.
 - [35] S. A. Hayward, Unified first law of black hole dynamics and relativistic thermodynamics, *Class. Quant. Grav.* 15 (1998) 3147–3162. arXiv:gr-qc/9710089, doi:10.1088/0264-9381/15/10/017.
 - [36] R.-G. Cai, L.-M. Cao, Unified first law and thermodynamics of apparent horizon in FRW universe, *Phys. Rev. D* 75 (2007) 064008. arXiv:gr-qc/0611071, doi:10.1103/PhysRevD.75.064008.
 - [37] M. Cruz, S. Lepe, J. Saavedra, A new approach to P–V phase transitions: Einstein gravity and holographic type dark energy, *Phys. Dark Univ.* 46 (2024) 101580. arXiv:2312.14257, doi:10.1016/j.dark.2024.101580.
 - [38] D. Kubiznak, R. B. Mann, P-V criticality of charged AdS black holes, *JHEP* 07 (2012) 033. arXiv:1205.0559, doi:10.1007/JHEP07(2012)033.
 - [39] L. N. Granda, A. Oliveros, Infrared cut-off proposal for the Holographic density, *Phys. Lett. B* 669 (2008) 275–277. arXiv:0810.3149, doi:10.1016/j.physletb.2008.10.017.
 - [40] M. Moresco, R. Jimenez, L. Verde, A. Cimatti, L. Pozzetti, Setting the Stage for Cosmic Chronometers. II. Impact of Stellar Population Synthesis Models Systematics and Full Covariance Matrix, *Astrophys. J.* 898 (1) (2020) 82. arXiv:2003.07362, doi:10.3847/1538-4357/ab9eb0.
 - [41] S.-L. Cao, X.-W. Duan, X.-L. Meng, T.-J. Zhang, Cosmological model-independent test of Λ CDM with two-point diagnostic by the observational hubble parameter data, *The European Physical Journal C* 78 (2018) 1–16.
 - [42] O. Farooq, B. Ratra, Hubble parameter measurement

- constraints on the cosmological deceleration–acceleration transition redshift, *The Astrophysical Journal Letters* 766 (1) (2013) L7.
- [43] S. R. Brownsberger, D. Brout, D. Scolnic, C. W. Stubbs, A. G. Riess, Dependence of Cosmological Constraints on Gray Photometric Zero-point Uncertainties of Supernova Surveys, *Astrophys. J.* 944 (2) (2023) 188. [arXiv:2110.03486](#), [doi:10.3847/1538-4357/acad80](#).
- [44] D. Brout, et al., The Pantheon+ Analysis: Cosmological Constraints, *Astrophys. J.* 938 (2) (2022) 110. [arXiv:2202.04077](#), [doi:10.3847/1538-4357/ac8e04](#).
- [45] D. Scolnic, et al., The Pantheon+ Analysis: The Full Data Set and Light-curve Release, *Astrophys. J.* 938 (2) (2022) 113. [arXiv:2112.03863](#), [doi:10.3847/1538-4357/ac8b7a](#).
- [46] M. Abdul Karim, et al., DESI DR2 results. II. Measurements of baryon acoustic oscillations and cosmological constraints, *Phys. Rev. D* 112 (8) (2025) 083515. [arXiv:2503.14738](#), [doi:10.1103/tr6y-kpc6](#).
- [47] M. Abdul Karim, et al., DESI DR2 results. I. Baryon acoustic oscillations from the Lyman alpha forest, *Phys. Rev. D* 112 (8) (2025) 083514. [arXiv:2503.14739](#), [doi:10.1103/2wwn-xjm5](#).
- [48] N. Aghanim, et al., Planck 2018 results. VI. Cosmological parameters, *Astron. Astrophys.* 641 (2020) A6, [Erratum: *Astron. Astrophys.* 652, C4 (2021)]. [arXiv:1807.06209](#), [doi:10.1051/0004-6361/201833910](#).